Desalination and Water Treatment
www.deswater.com

doi: 10.5004/dwt.2020.24962

179 (2020) 130–147
March

Evaluation of COD removal by biologically GSBR from photocatalytically pre-treated oilfield produced water

M. Golestanbagh[a,*], M. Parvini[b], A. Pendashteh[c]

[a]*Faculty of Chemical, Petroleum and Gas Engineering, Semnan University, P.O. Box: 148532-9862, Semnan, Iran, Tel. +98 9128404820/+982333383929; Fax: +982333383929; email: m.golestan@aol.com*
[b]*Faculty of Chemical, Petroleum and Gas Engineering, Semnan University, P.O. Box: 258963-3451, Semnan, Iran, Tel. +98 2144721405; email: m.parvini@semnan.ac.ir*
[c]*Environmental Science Department, Faculty of Natural Resources, University of Guilan, P.O. Box: 145368-3287, Rasht, Iran, Tel. +98 2155862481; email: msa_alz@yahoo.com*

Received 31 January 2019; Accepted 22 September 2019

ABSTRACT

Today combined photo-assisted advanced oxidation process (AOP) and biological processes are gaining in importance as treatment systems. The use of AOPs as a pretreatment step to enhance the biodegradability of produced water (PW) can be justified if the resulting intermediates are readily degradable by microorganisms in further biological treatment. Therefore, investigating the relationship between advanced oxidation pretreated effluent and subsequent bioreactor performance can help to optimize these systems. In this study, an integrated solar photoreactor – granular bioreactor was used to treat synthetic and real produced water. Solar photoreactor was designed and optimized using a cascade falling film theory and $TiO_2/SnO_2/CuO$ photocatalyst supported on the Scoria-concrete surface. The effects of various operational parameters on the photocatalytic process were investigated using response surface methodology (RSM). Optimum biochemical oxygen demand (BOD_5)/chemical oxygen demand (COD) ratio of 0.40 was achieved at pH of 6.5, a photocatalyst concentration of 60 g L^{-1}, temperature of 40°C, light exposure time of 70 min and H_2O_2 concentration of 2.5 mM. Photoreactor effluent with COD and BOD of 1,042 ± 10 and 432 ± 4 was fed into the aerobic granular bioreactor, respectively. The removed COD by the biological treatment was 50%, whereas by the combined photocatalytic–biological treatment it was reached to 94%. In the case of real produced water, the removal efficiency was decreased to 92%. Granule structure was determined using scanning electron microscopy. The combined biological–photocatalytic treatment significantly shortened the degradation and mineralization time of the biological treatment.

Keywords: Photoreactor; Bioreactor; Granular; Integrated; Produced water

1. Introduction

Water and energy are intrinsically linked and essential for human survival. However, along with the benefits, these fuels also adversely impact the environment during its production, distribution, and use. As oil and gas (O&G) are lifted to the surface, a significant amount of water is also brought along with it from the subsurface, which is known as produced water (PW). This is the largest volume of waste stream in the exploration and production process [1–3]. PW usually contains high concentrations of dissolved sodium chloride, dissolved hardness (calcium and magnesium carbonates), suspended solids, sulfate, aromatics and emulsified oils. Disposal of such large volumes of contaminated wastewater is a major issue especially with increasingly stringent environmental regulations [4–7]. The general nature of produced water production and composition as well as the

* Corresponding author.

environmental issues and current practices associated with the management of produced water streams are covered in several recent [4].

Since produced water contains several different contaminants with varying concentrations, therefore, numerous treatment technologies have been proposed for produced water treatment. The wide variety of produced water treatment methods have been reported previously [8–11]. Biological treatment of PW is an efficient, economical and environmentally friendly method. Due to the high concentrations of salts in produced water, halophilic microorganisms can survive in these hypersaline conditions [5]. The sequencing batch reactor (SBR) with aerobic granular sludge represents a good alternative to conventional activated sludge plants [12,13]. In particular, granular SBR systems guarantee high sludge settle-ability and excellent performance, with small space demand. The phenomenon of bio-granulation involves cell–cell interaction and includes physical, chemical and biological factors [14]. The products of this process are the biomass aggregates formed through the self-immobilization of micro-organisms [15]. More specifically, the granules are constituted by dense clusters containing millions of organisms per gram, including within them different bacterial species that play different roles in wastewater treatment [13]. Compared to conventional activated sludge flocs, the granules have a smooth texture, thick and very good settleability [16]. Further, the granular sludge can efficiently operate with high levels of organic load, high sludge retention times and variable operational conditions [12,15,17–21].

Biodegradation can completely mineralize the organics if they are not too recalcitrant or toxic. Recalcitrance and toxicity often are associated with complex aromatic structures and lack of specific enzymes in the microbial community [22]. A promising approach for treating recalcitrant and toxic organics is to combine an advanced oxidation process (AOP) with biodegradation [4]. The AOP can break the difficulty structures by free radical attack, which can generate readily biodegradable products. AOP, such as TiO_2 photocatalysis, has been considered as the most promising method for the remediation of contaminated water [23]. The efficiency of these systems is based on the production of strong oxidant species, such as hydroxyl radicals, which can oxidize almost all organic pollutants. For performing the photochemical reactions, various radiation sources, especially light sources, are available, such as gas-discharge lamps, glow lamps, fluorescent lamps or tubes, excimer radiators and lasers [24,25]. Each of these radiation sources has characteristic properties in terms of the type of the emitted spectrum and luminosity. The installation and operation of these methods are accompanied by such high costs that their use can be justified only in very special cases for economic reasons [26–28]. Instead of electrically operated light sources, solar radiation may also be used for performing photochemical reactions. However, in these systems challenging problems such as slow kinetics caused mainly by low photoefficiency need to be solved. An approach has focused on finding new catalysts able to work with band-gaps which coincide better with the solar spectrum [28,29]. Successful innovative catalyst compositions have been developed, but they have not been used in large-sized plants because no ''cheap'' solution has yet been developed. Many different solar photocatalytic reactors have been developed, such as parabolic-trough concentrator [30–36], thin-film-fixed-bed reactor [34], double skin sheet reactor [37] and compound parabolic concentrator (CPC) [38]. The CPCs are frequently researched based on its great advantages that the concentrator geometry allows indirect light to be reflected onto the absorber tube, not needing sun-tracking and that it is of high cost-effectiveness. Recently, a prototype of a flat-panel solar photoreactor was presented for wastewater treatment via solar illumination using TiO_2 nano-photocatalysts [39]. A significant increase in the efficiency of the scaled-up photoreactor was observed, which was shown by the faster decomposition of organic compounds. Casado et al. [40] described the critical role of the matching between the spectral distribution of the incident light and the absorption spectra of the semiconductor material on the accuracy of the simulation of solar photocatalytic reactors. The use of a sequence of two solar photocatalytic processes was investigated for the removal of copper, iron, zinc and ethylenediaminedisuccinic acid, used as a chelating agent, from real soil washing effluents [41]. Aoudjit et al. [42] presented the use of TiO_2 (P25) nanoparticles immobilized into a poly(vinylidene fluoride–trifluoroethylene) (P(VDF–TrFE)) membrane to assess the photocatalytic degradation of tartrazine in a solar photoreactor. Their results indicated the feasibility of the scale-up process for membrane solar photoreactors to degrade organic pollutants. The design and operation of a new solar photoreactor prototype named offset multi-tubular photoreactor (OMTP) are presented which addresses some of the limitations of current CPC solar reactors used in industrial wastewater treatment [43]. The OMTP increases the total treatment volume, the wastewater residence time, decreases the footprint and simplifies the reactor scale-up in comparison to the CPC. Abdel-Maksoud et al. [76] reported a TiO_2 water-bell solar photoreactor based on generating a thin water film to allow for solar light penetration and continuous oxygenation.

Apart from developments increasing the photocatalytic reaction rate, the most important progress in solar photocatalysis in recent years has been related to its combination with biological treatment and the application of toxicological analytical methods [44–46]. Both approaches have been successful in decreasing treatment time (i.e. plant size), which is another way of increasing overall process efficiency, in contrast to increasing the reaction rate itself [26–29]. Contaminant treatment, in its strictest meaning, is the complete mineralization of the contaminants; however, today photocatalytic processes only make sense for nonbiodegradable hazardous pollutants [28,47]. Baiju et al. [48] attempted to treat this wastewater by combining electro-Fenton (E-Fenton) and biological processes. The techno-economical evaluation of the coupling Fenton/biological system compared to the Fenton process as unique treatment showed that the lower oxidant uptake of the Fenton process for the coupling system is economically more profitable than using an excess of oxidant and a higher reaction temperature for the intensive Fenton process [49]. Chan et al. [50] demonstrate that the biodegradability of triazine-containing pollutants was significantly improved by the photocatalytic pre-treatment, and this proposed photocatalytic-biological integrated system can effectively treat various classes of

triazine-containing pollutants. Integration of biological process with photocatalytic oxidation for treating pharmaceutical wastewater characterized by the simultaneous presence of biodegradable and refractory compounds [51]. The study shows the integration of the two processes can be a promising technology. Wu et al. [52] proved that the combined biological-photocatalytic treatments provided a promising alternative candidate for the remediation of chlorothalonil-contaminated sites. When feasible, biological treatment is usually a good solution. Therefore, biologically recalcitrant compounds could be treated with photocatalytic technologies until biodegradability is achieved and then the water would be discharged to a conventional biological plant. Future evaluation of AOP efficiency should, therefore, be done from this perspective, instead of attempting to completely mineralize the contaminants using the OH radicals, which is always more expensive [53–55]. Such a combination reduces treatment time and optimizes the overall economics since the solar detoxification system can be significantly smaller [28]. Process kinetics make the first part of the photocatalytic treatment the quickest.

Low biochemical oxygen demand (BOD_5)/chemical oxygen demand (COD) ratio and high concentration of high molecular weight refractory organics being the typical characteristics of PW, makes physicochemical techniques a better option for their treatment. The use of AOPs as a pretreatment can be justified if the intermediates resulting from the reaction (more oxidized compounds, such as carboxylic acids, alcohols, etc.) are readily degraded by microorganisms. Although the treatment of PW effluents by the biological process has been investigated during the last years, only a few papers are based on actual PW. Moreover, to the best of our knowledge, there are no studies based on coupling AOP-biological systems for PW treatment. The feasibility of such a photocatalytic-biological process combination must always be considered, as it could mean a significant cost reduction due to the smaller solar collector field necessary. This research evaluates a novel reactor configuration for achieving intimately coupled photocatalysis and biodegradation. It is called the integrated photocatalytic-biological reactor, or integrated photocatalytic-biological reactor. $TiO_2/SnO_2/CuO$ was selected as the photocatalyst.

2. Methods

2.1. PW preparation

To determine the response of the integrated system under controlled conditions, synthetic PW was used during the whole study. Based on the halophilic medium proposed by other researchers [6,56] and real Maron oilfield produced water, produced water was simulated. The synthetic wastewater constitution total dissolved solids (TDS of 35,000 mg/L) in mg/L included: NaCl 31,173; $CaCl_2{\cdot}2H_2O$ 60; KCl 2000, $MgCl_2{\cdot}6H_2O$ 50; $NaHCO_3$ 800, KH_2PO_4 100. The composition of the wastewaters gave a C/N/P ratio of approximately 100/10/1 by adding NH_4Cl and KH_2PO_4. The pH was adjusted to 7 using NaOH. All of the chemicals used in this study were of technical grade. Crude oil was collected from Iranian oilfields. Synthetic produced water was prepared in a homogenizer (T 25 digital ULTRA-TURRAX) by mixing salts and crude oil in a 5 L polyethylene container for 24 h (2,400/min) to achieve equilibrium between the oil and water phases [56]. BOD_5 and COD and of synthetic PW (1 mL oil/L) were 450 and 2,050, respectively. BOD_5 and COD of synthetic PW were selected based on their highest value in real PW.

Real produced water samples were transported to the laboratory and stored at 4°C until their utilization. All samples were thawed before treating. The characteristics of the produced water are given in Table 1. The wastewater pH was adjusted to 7 using HCl before feeding to the fermenter. NH_4Cl and KH_2PO_4 were added as supplementary nutrients.

2.2. Solar photocatalytic study

As the raw PW collected from the plant is not effectively consistent with biological degradation, it was pretreated with solar photocatalytic method. The visible-light-driven photocatalysts were $TiO_2/SnO_2/CuO$ nanocomposite (surface area >267 m^2/g, crystallites mean size 40–50 nm). The molar ratio of Sn(Cu) to Ti was 0.15°C and calcined at 550°C. The optical absorption edges of the nanocomposite located in 500 nm, corresponding to a band gap energy (Eg) of approximately 2.31 eV. The inconvenience of suspension approach at large scale is the catalyst-recovering step from the solution at the end of the operation. This problem has be solved

Table 1
Water quality analysis of real oilfield produced water (average ± standard deviation; n = 10)

Parameter		Parameter	
pH	8.2 ± 0.2	PO_4^{3-}	40.6 ± 3.1 (mg/L)
Turbidity	150 ± 15 (NTU)	Al	0.01 ± 0.002 (mg/L)
TDS	48,200 ± 560 (mg/L)	Sn	0.32 ± 0.12 (mg/L)
COD	1,380 ± 210 (mg/L)	Ca	18.2 ± 0.5 (mg/L)
O&G	16 ± 1.2 (mg/L)	Mg	3.6 ± 0.6 (mg/L)
Total organic carbon (TOC)	562 ± 18 (mg/L)	Cd	0.01 ± 0.001 (mg/L)
Suspended solids (SS)	171 ± 12 (mg/L)	Cu	0.04 ± 0.009 (mg/L)
Volatile suspended solids (VSS)	79 ± 6 (mg/L)	Total Cr	0.004 ± 0.001 (mg/L)
Ammonia-N	11.5 ± 1.3 (mg/L)	Hg	0.65 ± 0.05 (mg/L)
Total phenols	85 ± 0.25 (mg/L)	Ba	4.2 ± 0.3 (mg/L)
Sulfide	2.6 ± 0.4 (mg/L)	Ni	0.08 ± 0.00 (mg/L)

immobilizing the catalyst on Scoria-concrete surface without activity losses using epoxy concrete sealer [57,58]. The photo-reactor was composed of 4 horizontal and 3 inclined (45°) concrete bed covered with a Pyrex sheet to strongly limitate water evaporation which could induce errors in concentrations. The deposited photocatalyst was laid on the 7 beds of the photoreactor, which corresponded to a surface of 0.1484 m^2 to prepare efficient contact time between photocatalyst and PW. The photoreactor, with a solar radiation-collecting surface, is mounted on a fixed rack inclined at an angle equal to the local latitude (37° for Tehran). The PW flows at 220 L/h directly from one step to another and finally into a tank. Photo catalyst dosage was fixed on 60 g/m^2. The effluent flowed down on the steps before being collected in a tank, from which it was elevated to the top of the steps for recirculation. The flow was distributed by a pipe with 1 cm mesh size over the first step. The reactor hydraulics parameters were controlled by water depth limited to 3.2 mm. Dissolved oxygen (DO) and pH were monitored in all the experimental period time by Aramis-2010 and HI2002-01, respectively. Prior to measurement, the liquid samples were centrifuged with Sigma 101 at 2,500 g for 10 min to remove the detached solid particles. Solar ultraviolet (UV) and visible radiation has been determined during the experiments. A global UV/Vis radiometer (PMA2123, 400–700 nm) was used mounted on a 37° fixed-angle platform (the same angle as the photoreactor). The other sensor for the direct visible light (International Light-ESD 400, Germany) is mounted on a sun tracking platform. These sensors provide data in terms of global or direct UV/Vis solar energy power incident per unit area. Obviously, solar-UV power varies during experiments, made still more noticeable by clouds. This gives an idea of the energy reaching any surface in the same position with regard to the sun. Normalized irradiation time was calculated based on the method presented by Malato et al. [26,28]. The schematic of the photoreactor was presented at Fig. 1. The details of photoreactor are listed in Table 2.

2.2.1. Experimental design and mathematical modeling

Design of experiments response surface methodology (RSM) was used to evaluate the effects of different variables on ceiling fan performance. It not only shows the optimum conditions, but it also proposes fitted regression models. The central composite design (CCD) under RSM was used to characterize the interaction between the process variables and the response. Preliminary experiments were performed for the determination of the independent variables and their experimental ranges to design the experimental runs. Based

Table 2
Photoreactor parameters

Total length of the photoreactor	m	60
Total height of the photoreactor	m	50
Beds dimension (horizontal/inclined)	m	10 × 20 × 5/11.4 × 20 × 5
Bed porosity	%	0.22
Inclined beds slope	deg	45°
Number of beds		7
Total area of beds	m^2	0.1484
Total photocatalyst loading	g/m^2	60
Total photocatalytic zone volume	L	0.410
Storage tank volume	L	6
Aeration rate	L/h	250
Circulation rate	L/h	220

Fig. 1. Experimental solar photoreactor.

on the literature and the preliminary results, the four most important operating variables, which affect the efficiency of a photocatalytic process are pH (A), irradiation time (B), photocatalyst dosage (C), temperature (D) and H_2O_2 concentration (E). These parameters were considered as the system independent variables and COD removal efficiency was calculated as the process response. BOD_5/COD was considered as the dependent variable (responses). Table 3 shows the experimental design based on CCD used in this study.

A set of 50 experimental runs, including duplicates were designed using CCD. The results were analyzed using Design Expert 8.0 and a regression quadratic polynomial model was proposed as follows:

$$Y(\%) = \alpha_0 + \sum \alpha_i X_i + \sum \alpha_i X_i^2 + \sum \alpha_{ij} X_i X_j + \varepsilon \quad (1)$$

where α_0 is the constant coefficient, α_i, α_{ii} and α_{ij} are the regression coefficient and X_i, X_j indicates the independent variables. ε represents the random error. All statistical analyses were carried out using Design Expert 8.0. The comparison of responses between those predicted by the model and those measured by simulation was conducted using Student's *t*-tests, while all responses in the central points were pooled after conducting Levene's test for homogeneity of variances, and then compared using a Student's *t*-test. After performing a sensitivity analysis, the process was optimized. The optimized biological ratio obtained through the software (Design Expert 8.0) was compared by experimental measurement at optimum condition.

2.3. Biological reactor

Hypersaline soil from Kazar, the Persian Gulf and Urmia seaside in Iran served as a source of tropical halophilic microorganisms. The isolation of microorganisms capable of degrading crude oil in produced water began by placing approximately 6 g of soil into 200 ml of synthetic produced water [7]. After 15 d of mixing on a shaker table (150/min, 30°C), a 2 ml sample of the mixture was then transferred to a fresh medium. After three repeated steps of the process, the resulting mixture was free of soil [5,56].

A glass airlift reactor with a working volume of 5 L was used. The internal diameter of the down-comer was 80 mm. The riser had a height of 800 mm and an internal diameter of 400 mm, and it was at 2 cm from the bottom of the downcomer. The hydraulic retention time was 8 h. Fig. 1 depicts the experimental set-up. Compressed air was supplied through an air diffuser placed at the bottom of the reactor. The reactor was equipped with DO (Crison DO 6050, USA) and pH probes (Crison pH 5333, USA) that were connected to a data monitoring system (Crison Multimeter 44, USA). The temperature in the reactor was maintained using a temperature controller coupled with a belt-type heating device (Horst, Germany). The pH of the reactor was maintained by a regular addition of $NaHCO_3$ into the reactor. Feeding to the reactor was made with a membrane pump (ProMinent Gamma-L). Air flowrate in the reactor was regulated by a mass-flow controller (Aalborg, USA) with a range of 125–500 mL min^{-1}. Samples were regularly withdrawn from the effluent and filtered through a 0.20 μm syringe filter driven unit from Millipore: Merck (Germany) provided with a high-density polyethylene housing and membrane of hydrophilic Durapore prior to analysis. The operational conditions in the reactor during the experimental period were: Temperature of 16°C–30°C, DO of 2–5 mg/L and pH of 7–8. Fig. 2 shows the schematic of the bioreactor.

The reactor was operated in successive cycles of 6 h each. One cycle consisted of 3 min influent addition, 305 min aeration, 30 min settling, 7 min effluent discharge, and 15 min effluent withdrawal. Effluent was withdrawn at 50 cm from the bottom of the reactor. The settling time was chosen such that only particles with a settling velocity larger than 10 m/h were effectively retained in the reactor. Influent and effluent pH and electrical conductivity were routinely measured. All experiments were carried out based on standard methods for water and wastewater experiments [59]. The reactor was operated for one month at a constant temperature of 30°C.

The sequencing batch airlift reactor was inoculated with and was fed with PW as the carbon and energy source to promote the granulation process. The initial mixed liquor suspended solids (MLSS) was about 3,000 mg/L. Small granules could be seen after 15 d of the start-up and at the end of 1-month stable granules were observed. The granules increased in diameter and adopted an irregular shape. Scanning electron microscopy (SEM) was used to determine granule characteristics. Before scanning, granules were placed in 3% glutaraldehyde overnight and washed with phosphate buffer and then frozen using liquid nitrogen. Furthermore, granules were dewatered by placing in 30%, 50%, 70%, and 100% ethanol and then coated with gold.

2.4. Integrated photocatalytic biological degradation study

Since the effluent is not convenient for biological degradation, pretreatment is necessary. From the literature, it

Table 3
Experimental design factors

Name	Units	–1 Level	+1 Level	–α	+α
pH		5.5	8.5	4	10
Photocatalyst dose	g/m^2	35	60	22.5	72.5
Time (visible light)	min	90	180	45	225
Temperature	C	25	45	15	55
H_2O_2	mM	2.5	7.5	0	10

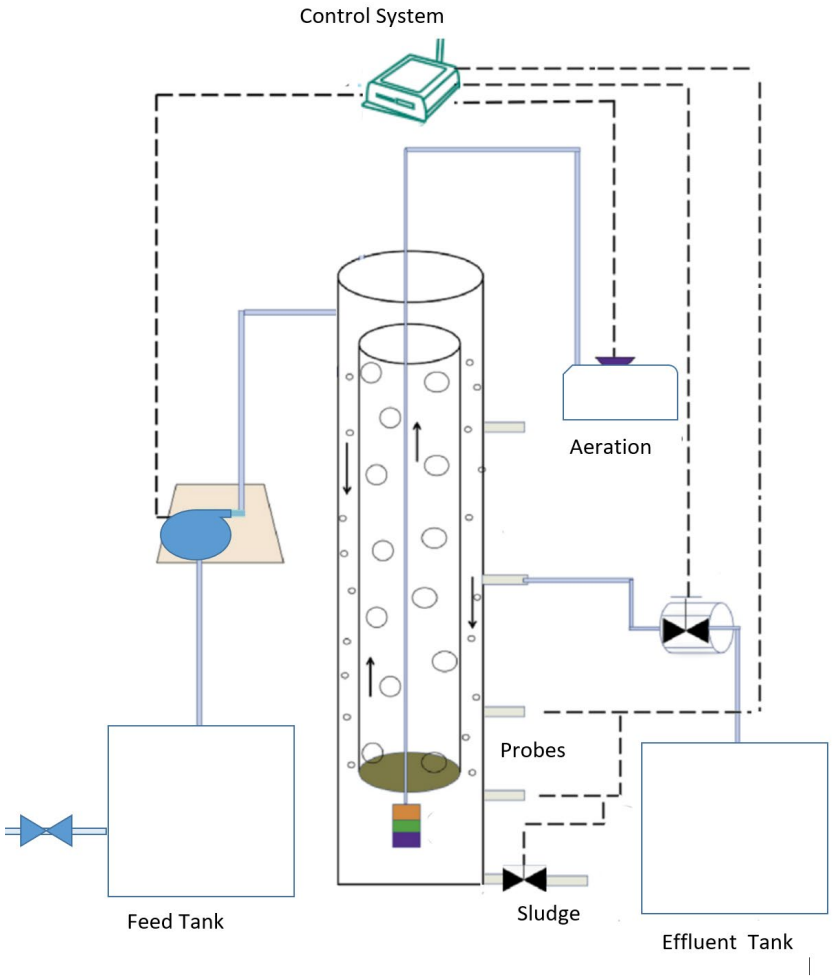

Fig. 2. Schematic of solar bioreactor.

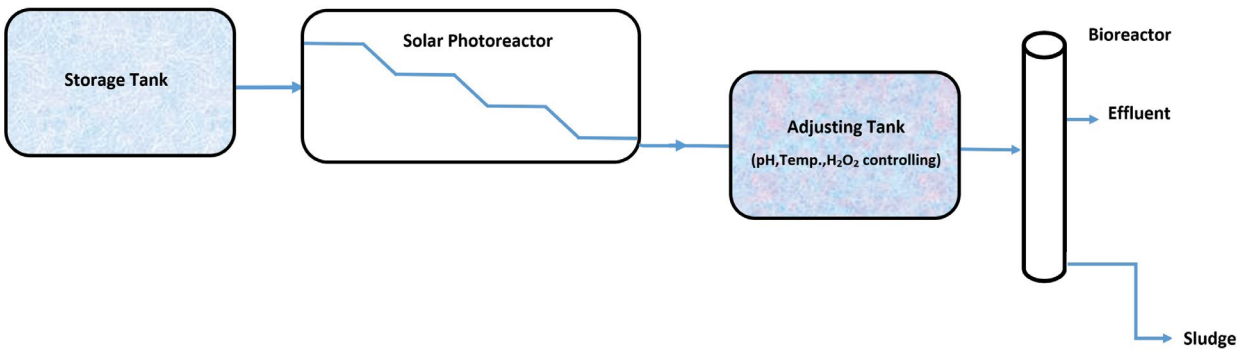

Fig. 3. Schematic of integrated photoreactor – bioreactor.

is understood that solar photocatalytic treatment has given the best results [28]. Because of this, the solar pre-photocatalytic and biological treatments are conducted sequentially as shown in Fig. 3. The PW flowed into the photoreactor by the circulative mode and the effluent was passed through a filter to the bioreactor with the valve open. The operational condition of the photoreactor was set to optimum condition.

About 2 mL of the effluents that flowed from the bioreactor and the photoreactor were withdrawn at timed

intervals and immediately filtered using a syringe equipped with a disposal filter having a pore size of 0.2 m. The COD of the samples was determined according to the Freire and Sant'Anna [60,61] method. MLSS, mixed liquor volatile suspended solids, BOD, TDS and O&G were measured according to the standard methods [62]. To identify the present organic compounds in the PW and determine the efficiency of degradation under optimum condition, 250 ml samples of wastewater were taken before and after treatment under optimum condition and analyzed using a 7890A, Agilent Technologies (HP, USA) gas chromatography (GC) coupled to 5975C, Agilent Technologies (HP, USA) mass detector (MS). The extraction procedure for wastewater samples was manual separatory funnel liquid–liquid extraction as described in US EPA SW-846 Method 3510C (EPA, 1996) [59]. The column used for detecting the organic compounds by GC-MS was HP-5 MS column of 30 m length, 0.25 mm inner diameter, and 0.25 mm film thickness. An injection volume of 1 mL with a splitless capillary injection system was used for the analysis of samples.

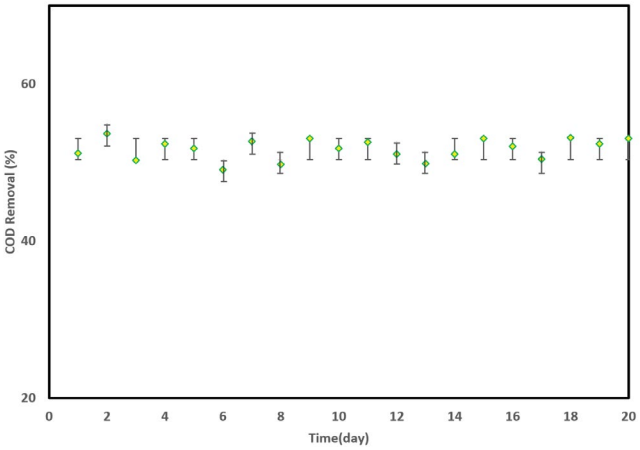

Fig. 4. COD removal of bioreactor before PW pretreating.

3. Results and discussion

In preliminary experiments, to examine the effect of adsorption of pollutants by Scoria and "photocatalyst, experiment was conducted both in the absence (dark condition) of light. The effects of adsorption on COD removal and BOD_5/COD at pH of 6.0, temperature of 35°C and time of 70 min (Fig. 4) were investigated. Experimental data showed low COD removal of 2% and 6.2% were obtained in the absence of light for Scoria and photocatalyst, respectively. However, when the temperature increased from 25°C to 45°C under the same aforementioned conditions, there was no significant change in the COD removal efficiency. The reason for low removal efficiency in the absence of light may be due to either very low adsorption of organic pollutants by the photocatalyst particles or the volatility of a part of light hydrocarbons due to the airflow. In subsequent experiments, the COD removal of about 3.8% was achieved in the presence of light and absence of photocatalyst under the above condition". The results indicate that photodegradation plays a more important role than the adsorption process. All these results suggested that both light and photocatalyst are needed for effective treatment of PW.

3.1. Biological treatment

Raw and treated wastewater samples with Fenton applications were subjected to biological degradation. The results of the physicochemical analysis indicate that the collected PW sample contains high organic load as represented by high BOD_5, COD values, chlorides, and sulfates. One more significant point was the high conductivity of samples, related to the presence of a large number of chloride ions. A batch control test of PW with only biological treatment confirmed only 50% ± 3.4% degradation results (Fig. 5). The biodegradability index (BOD_5/COD) was 0.3, indicating that raw PW was directly amenable to biodegradation. As our main goal was to achieve maximum degradation of organic matter present in the PW, therefore, the sample was

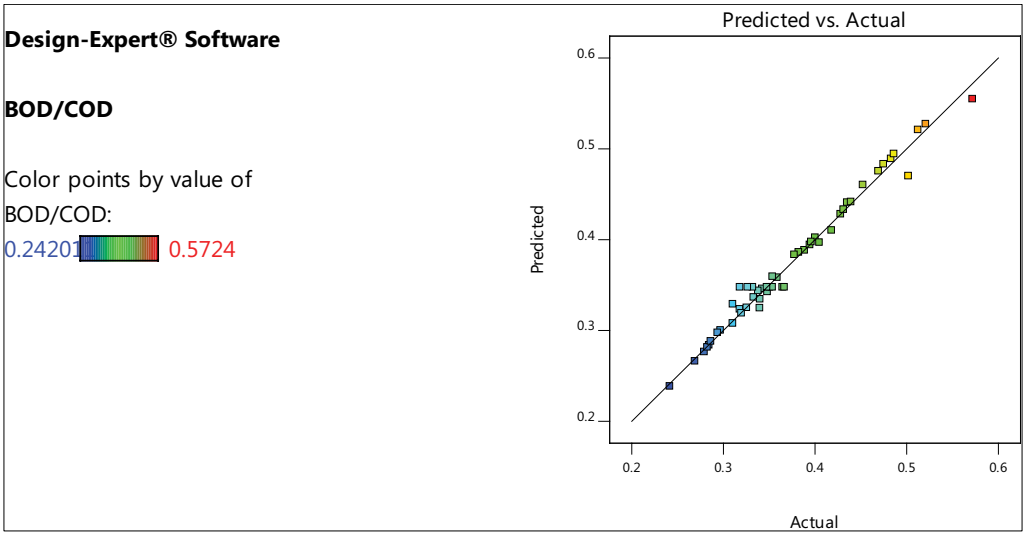

Fig. 5. The predicted vs. actual plots of the response.

subjected to independent photoreactor as a pre-treatment technology to achieve the enhanced degradation of organic content of PW.

3.2. Photocatalytic treatment

3.2.1. RSM approach

The RSM-CCD approach is used to design the experiments, evaluate the effect of the process parameters, identify the optimum conditions, and build a regressive model. The efficiency of the photocatalytic process was evaluated based on the COD and BOD_5 removal from the PW. A polynomial regression equation was developed by using CCD design to analyze the factor interactions. The best fitted quadratic polynomial regression model was obtained as follows:

$$\begin{aligned} BOD_5/COD = {} & 0.347 - 0.0136A + 0.0643B + 0.0353C \\ & + 0.0189D + 0.0092E - 0.0006AB \\ & - 0.0045AC - 0.0009AD + 0.0064AE \\ & + 0.0052BC - 0.0005BD - 0.0009BE \\ & - 0.0004CD - 0.005CE - 0.0001DE \\ & + 0.0055A^2 + 0.0196B^2 \\ & + 0.0129C^2 + 0.0062D^2 - 0.0103E^2 \end{aligned} \quad (2)$$

In this equation, the coefficients with positive and negative signs meant that those have a synergistic or antagonistic effect on the photocatalytic process.

3.2.2. Statistical analysis

A statistical analysis of variance (ANOVA) based on CCD was performed to determine the fitness and significance of the model shown in Table 4. In the quadratic model, the *F*-value of 78.13 and *p*-value of <0.0001 show that the model is statistically significant, at which *p*-value should be less than 0.05 for a model term to be significant. Lack of fit (LOF) shows the variation in the data around the fitted model and compares residual error with pure error [63,64]. In our case, LOF indicates the variation of data around the fitted model ($p > 0.05$ for all responses). Also, according to ANOVA, the effect of variables and interaction between them follows the following order: Time (B) > pH (A) > H_2O_2 concentration (D) > Temperature (C) > AB interaction > AC interaction. The predicted coefficient of designation value (R^2) was 0.971 which is very close to the corresponding adjusted R^2 value of 0.945. The high value of R^2 shows that the quadratic polynomial equation can predict degradation efficiency in the experimental range [64].

Fig. 5 shows the plot of predicted value vs. the observed values in COD degradation, at which with respect to our

Table 4
Response surface methodology (RSM), central composite design (CCD), and analysis of variance (ANOVA)

Source	Sum of squares	*df*	Mean square	*F*-value	*p*-value	
Model	0.2672	20	0.0134	78.13	<0.0001	significant
A-pH	0.0073	1	0.0073	42.98	<0.0001	
B-Time	0.1654	1	0.1654	967.36	<0.0001	
C-Dose	0.0497	1	0.0497	290.80	<0.0001	
D-Temperature	0.0143	1	0.0143	83.91	<0.0001	
E-H_2O_2	0.0034	1	0.0034	19.60	0.0001	
AB	0.0000	1	0.0000	0.0674	0.7970	
AC	0.0007	1	0.0007	3.83	0.0601	
AD	0.0000	1	0.0000	0.1645	0.6881	
AE	0.0013	1	0.0013	7.55	0.0102	
BC	0.0009	1	0.0009	5.15	0.0308	
BD	7.220E-06	1	7.220E-06	0.0422	0.8386	
BE	0.0000	1	0.0000	0.1645	0.6881	
CD	4.500E-06	1	4.500E-06	0.0263	0.8723	
CE	0.0008	1	0.0008	4.60	0.0406	
DE	3.200E-07	1	3.200E-07	0.0019	0.9658	
A^2	0.0010	1	0.0010	5.69	0.0239	
B^2	0.0123	1	0.0123	72.07	<0.0001	
C^2	0.0054	1	0.0054	31.38	<0.0001	
D^2	0.0012	1	0.0012	7.14	0.0123	
E^2	0.0034	1	0.0034	20.00	0.0001	
Residual	0.0050	29	0.0002			
Lack of fit	0.0028	22	0.0001	0.4019	0.9518	not significant
Pure error	0.0022	7	0.0003			
Corr. total	0.2722	49				

findings, there is a good agreement between the predicted and experimental values. In addition, the normal probability plot of the residuals, as shown in Fig. 6, shows that the distribution of the obtained data is almost linear.

A perturbation plot shows the comparison among the effects of all the factors at a particular point in the design space. The perturbation plot for the COD and BOD_5 photodegradation process is shown in Fig. 7. Removal was plotted by means of changing only one factor over its range while keeping other factors constant. The plot gives the effects of all factors at the central point. The curvature of "B" and the slope of the "A and C" line indicate that the response is sensitive to these factors.

3.2.3. Effect of process variables on BOD_5/COD

The effects of interactions between variables in the photocatalytic process of COD removal using the two and three-dimensional surface-response plots obtained from the quadratic model can be discussed based on the

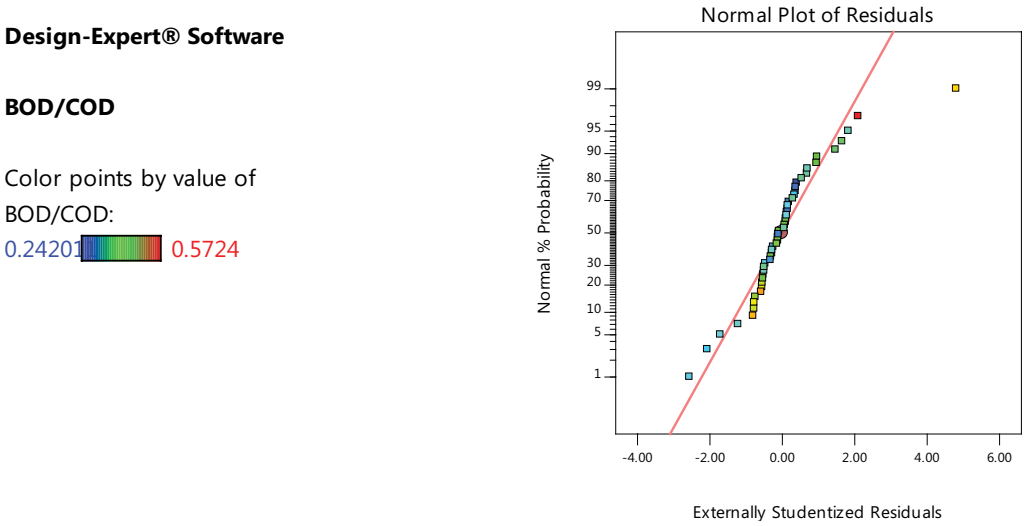

Fig. 6. Normal probability plots of the response.

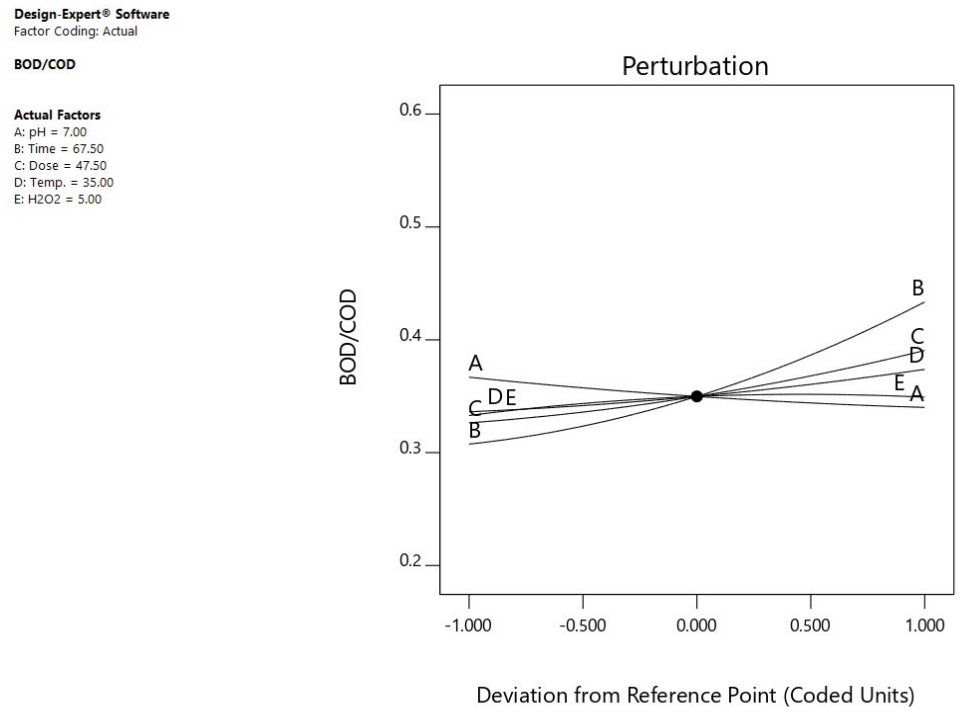

Fig. 7. Perturbation plot of affecting factors.

analyses, as shown in Figs. 8–11. Figs. 8 shows the simultaneous influence of initial pH and temperature on the BOD_5/COD ratio. The pH value plays an important role in photocatalyst surface charge, the mechanism and the rate of hydroxyl radical generation [65] and consequently on the rate of photocatalytic degradation of organic pollutants [66]. At a specific pH value, an organic compound can attain a positive or negative charge, as well as the neutral form in PW. Electrostatic interaction between photocatalyst surface, organic molecules and formation of charged radicals during the photocatalytic oxidation is strongly dependent on the pH of PW [67]. According to the literature, different organic materials have different activity in the photocatalytic degradation process. Some organic materials are posed on fast degradation under acidic conditions, while others are degraded faster at higher pH, so it is important to

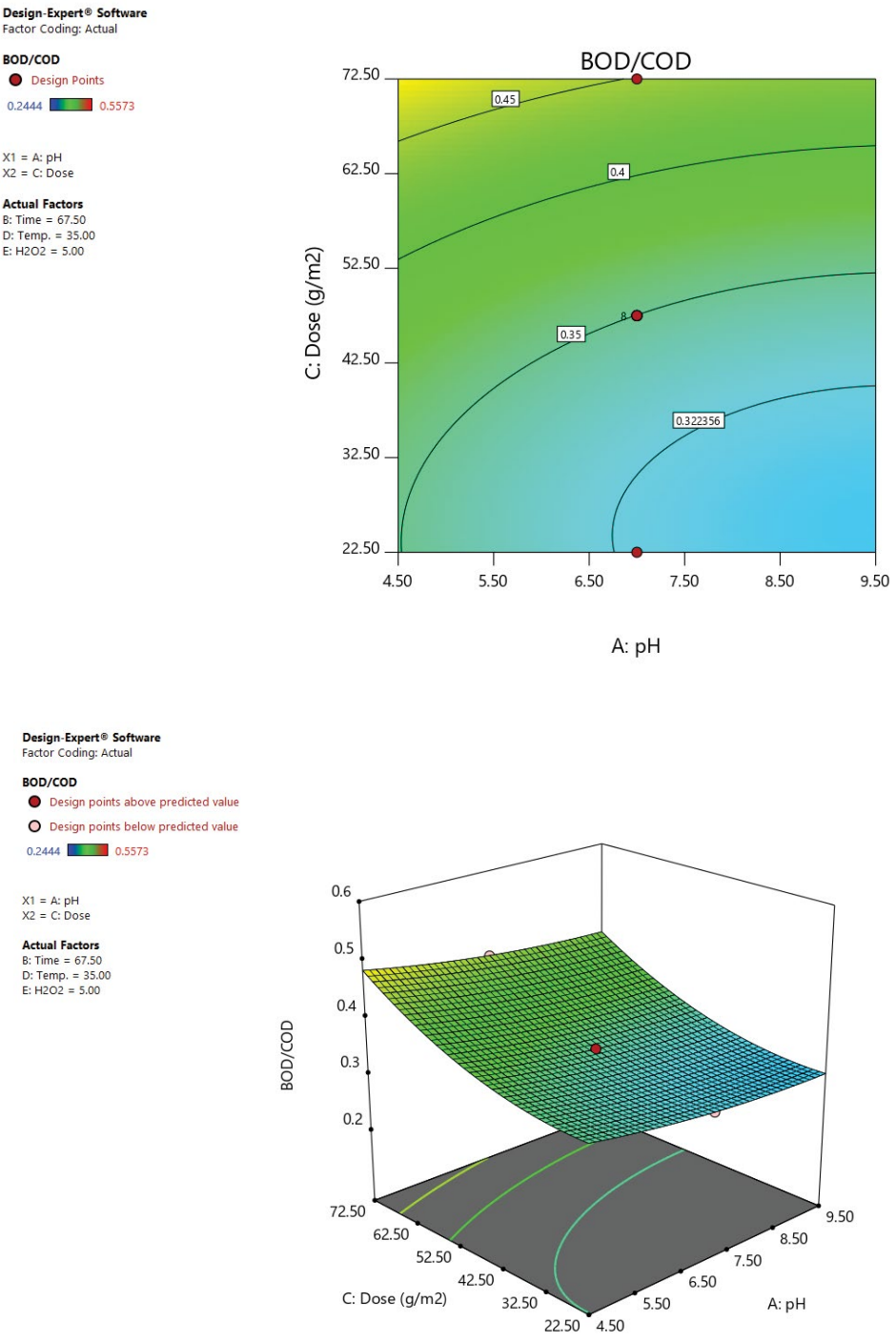

Fig. 8. Effect of pH and photocatalyst dose on BOD_5/COD ratio in photoreactor.

determine the optimum pH for photocatalytic degradation [67]. From this figure, the pH had a strong reverse effect on the response and the ratio was increased with a decrease in pH value. The effect of pH on the photocatalytic reaction can be argued with the help of the point of zero charge of photocatalyst [65] and the adsorption of the pollutants on the photocatalyst in different pH value [68,69]. The point of zero charge (pzc) of photocatalyst is at pH~6.3. The surface of the photocatalyst is protonated under acidic conditions (pH < 6.3), whereas it is deprotonated under alkaline conditions (pH > 6.3). Depending on the anionic or cationic form of the organic compound, the photodegradation efficiency was enhanced or inhibited by the electrostatic attraction or repulsion, respectively between the photocatalyst's surface and the organic molecule [66]. Moreover, protonation and deprotonation of the organic contaminants can happen depending on the solution pH. In addition, under Vis-light, the composite produces OH radicals, which in turn may

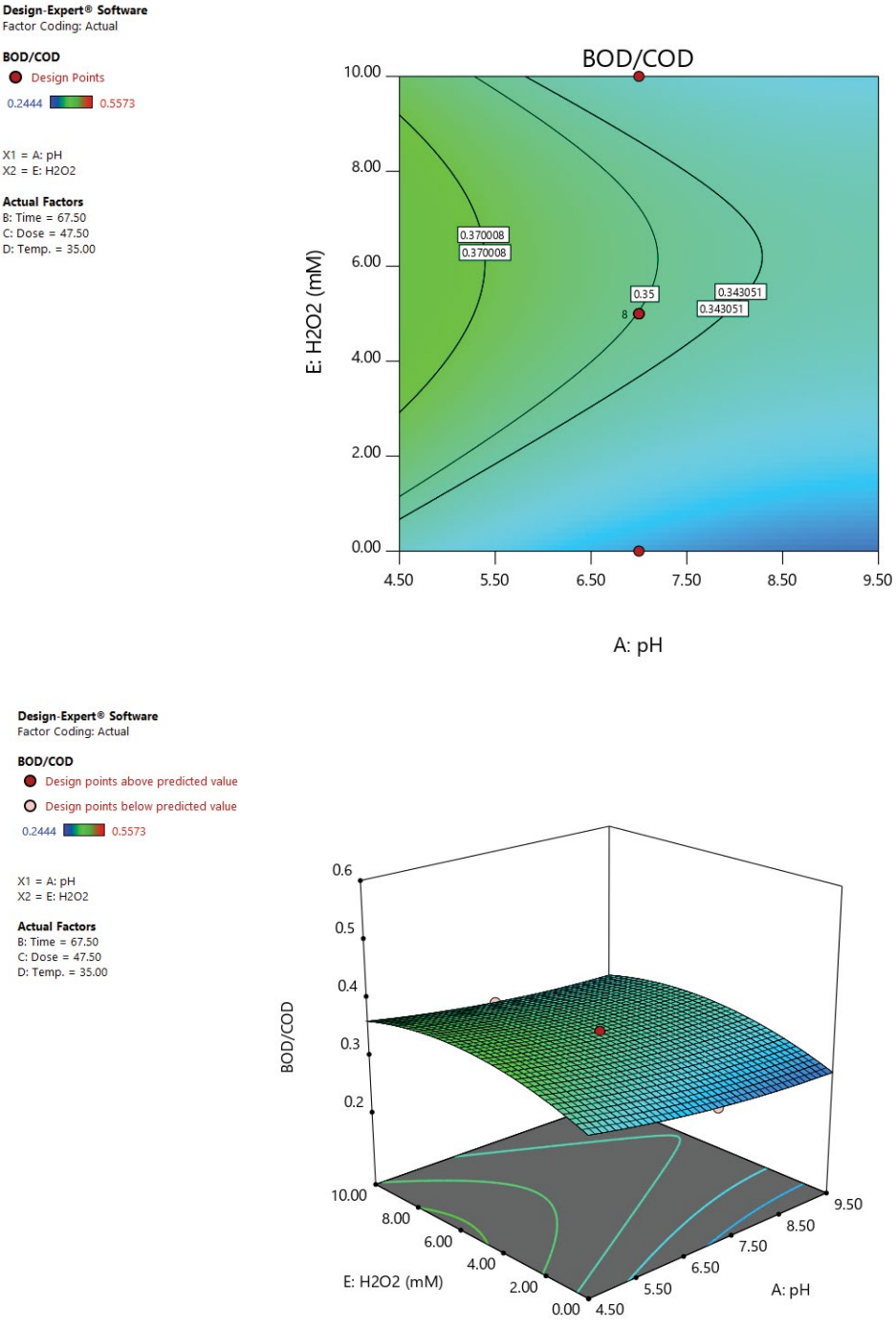

Fig. 9. Effect of pH and H_2O_2 interaction on the BOD_5/COD ratio in photoreactor.

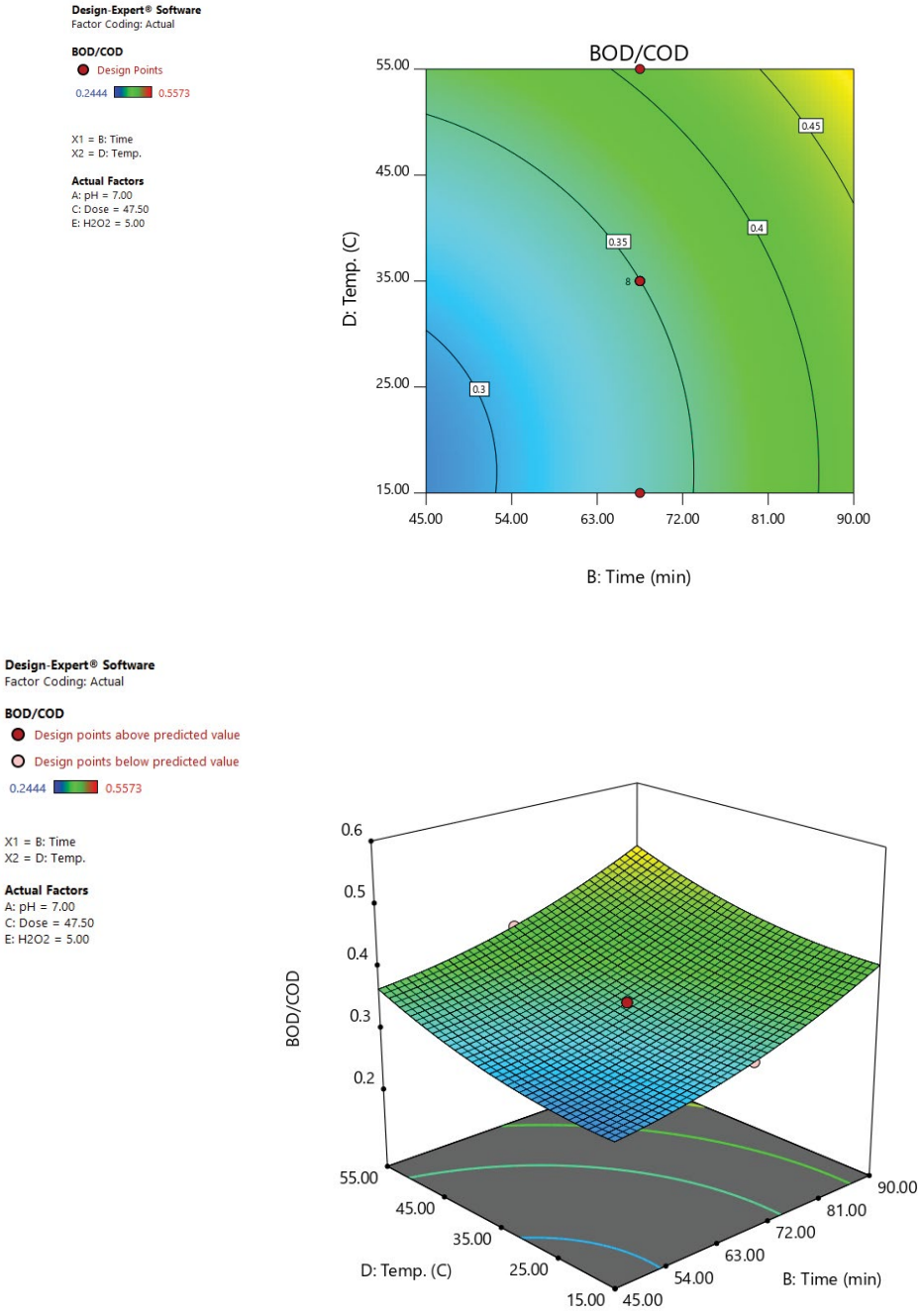

Fig. 10. Effect of temperature and time interaction on BOD_5/COD ratio in photoreactor.

increase the reaction rate in acidic conditions [70] while in a strongly alkaline environment such radical species are rapidly scavenged and the reaction rate decreases. In the present study, the process of increasing BOD_5/COD was favored by the protonated surface of photocatalyst. The maximum BOD_5/COD was achieved at pH values around 4.5 due to strong electrostatic attraction between the cationic photocatalyst and anionic organic pollutants. Fig. 8 is used to determine the amount of BOD_5/COD via various catalyst values in different pH values. Based on the figure, the photocatalyst dosage has a synergetic effect on organic compound degradation. Increasing photocatalyst content on rector beds results in increasing radical generation rate which leads to COD reduction. The more photocatalyst the more electron-hole production and as a result, higher content of PW can be decomposed. As shown, the interaction of pH and catalyst dose factors has a synergistic effect at higher catalyst dosage and lower acidic pHs. This agrees with the coefficients in Eq. (2), because pH has a minus sign confirming an increase in pH decreases the response while catalyst dosage has a plus sign, confirming an increase in the catalyst dosage has a synergistic effect on the response.

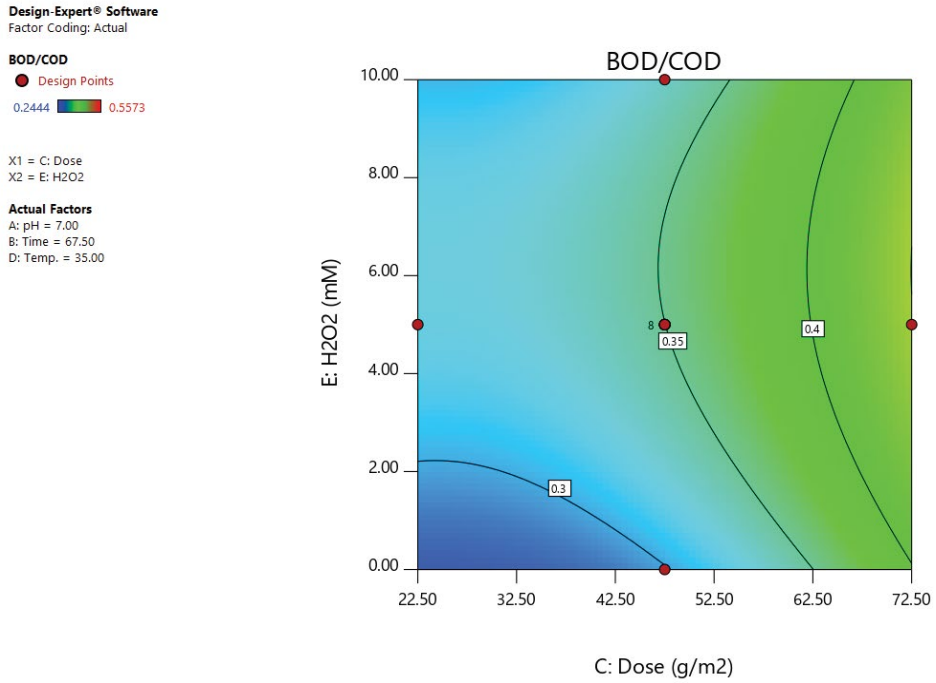

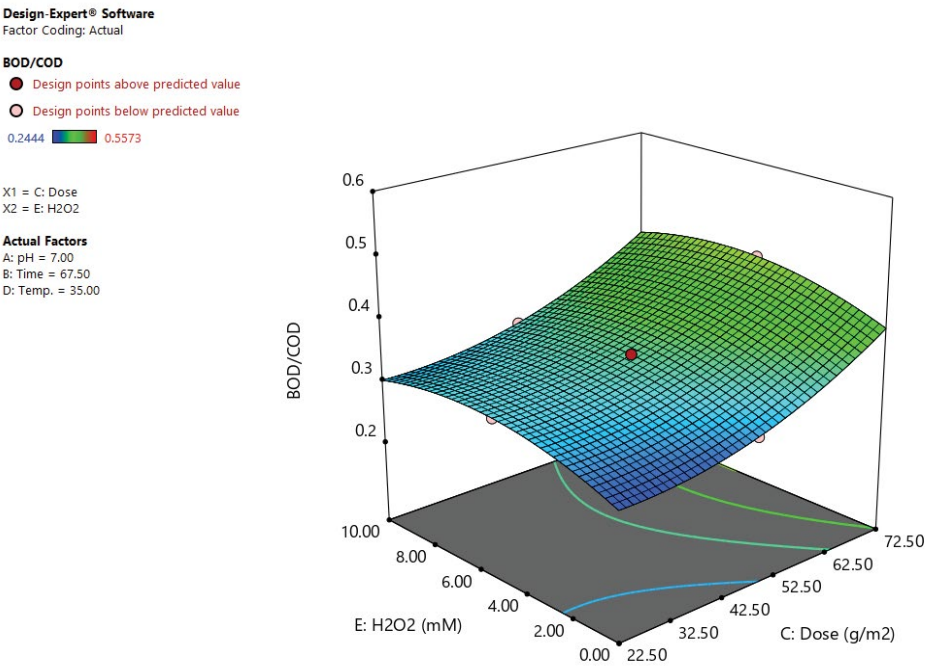

Fig. 11. Effect of H_2O_2 and photocatalyst dose on BOD_5/COD ratio in photoreactor.

Fig. 9 shows the interaction effect of pH and H_2O_2 concentration on COD and BOD_5 removal efficiency, while the other variable was set at the middle value. From Fig. 9 it is observed that the reduction percentage of COD and BOD_5 in aqueous solution depends dominantly on H_2O_2 concentration. At a constant pH, increasing the H_2O_2 concentration up to 6 mM leads to increase COD degradation and the further increase has an inverse outcome on the process. This behavior is proof of the existence of an optimal dosage in H_2O_2. It must be underlined the fact that hydroxyl radicals produced upon photolysis of hydrogen peroxide can react with organic molecules, but also with an excess of H_2O_2 [71–74]. At low hydrogen peroxide concentrations, the formation of OH radicals is the kinetic determining step. H_2O_2 cannot generate

enough hydroxyl radicals and the oxidation rate is logically slow. Further, most free radicals are directly consumed by organic matters [73]. In the presence of a high concentration of peroxide, we could expect that more OH radicals would be produced. However, these radicals preferentially react with the excess of H_2O_2 [75]. This undesirable reaction competes with the destruction of the organic compounds. The interaction of pH and H_2O_2 concentration showed that the best degradation efficiency can be achieved at moderate H_2O_2 concentration in acidic solution. In the acidic environment, due to increased H^+ production, the equilibrium of the environment was lost, and H^+ was trapped by radical hydroxyl according to the following reactions. This results in a reduction in the amount of organic compound degradation.

$$H_2O_2 \rightarrow 2H_2O + O_2 \quad (3)$$

$$H_2O_2 \rightarrow O_2 + 2H^+ + 2e^- \quad (4)$$

$$^{\bullet}OH + H^+ \rightarrow H_2O \quad (5)$$

Fig. 10 shows the interaction effect of temperature and exposure time, while the other variable was set at the middle value. This figure shows that an increase in the removal efficiency of the COD with a simultaneous increase in temperature and visible light exposure time. Fig. 5 shows that time as an important parameter has a positive effect on degradation efficiency. This can be attributed to the fact that the production of conduction band electron-valence band hole pairs (e^-_{CB} + h^+_{VB}) and consequently hydroxyl radicals' generation increased with increasing irradiation time and more attack of hydroxyl radicals lead to an ascent in COD and BOD_5 removal amount. In addition, The figure shows that a part of organic compound degradation was favored by increasing temperature. This is due to the transfers of photocatalyst electron in valance bond to higher energy levels and hence facilitating the production of electron-hole pair. It is well known that photochemically induced reactions often have a low activation energy.

Fig. 11 displays the 2D and 3D surface plots of the response as a function of catalyst dosage and H_2O_2 concentration. As can be seen, the two factors follow similar trends, an increase in the catalyst dosage and the H_2O_2 concentration increases the COD degradation. The influence of the catalyst dosage on the degradation process is more considerable than the H_2O_2 concentration. Given that, high catalyst loading is neither economical nor efficient. At a low dosage, H_2O_2 slightly increased COD degradation; however, it has a more pronounced effect at higher levels for the catalyst dosage. Lower H_2O_2 concentration needs more catalyst dosage. At low dosages of H_2O_2, less hydroxyl radicals were probably generated, being insufficient for the degradation reaction. The increase in the initial dosage of hydrogen peroxide increased the concentration of $^{\bullet}OH$ radicals and improved the oxidation process up to a certain limiting dosage.

3.2.4. Optimization and validation

To determine the optimum conditions for the photodegradation process, the optimization tool of Design-Expert® was utilized. To achieve the optimum conditions, all the factors were selected within the range while BOD_5/COD was defined between 0.4–0.5. However, comprehensive optimization is the one that accounts for the economic aspects of a process along with maximizing its efficiency. Among several optimum conditions, the one with the minimum exposure time is recommended. Accordingly, the optimum process variables and the related response are presented in Table 5. To check the accuracy of the optimization, the model was validated by conducting photocatalytic degradation under the optimum conditions. The experimental and the predicted results in Table 5 are in excellent agreement, which verifies the model validation in a 95% confidence interval.

3.3. Combined photocatalytic – biological treatment

At the end of 90 min of photocatalytic treatment, the COD of PW had reduced from 2,050 mg/L to 1,042 ± 10 mg/L, and the BOD_5/COD ratio had increased from 0.21 to 0.40. Based on the Environment Protection Act (Ministry of Environment and Forest, 1986) [59] for any trade effluent to be discharged into inland surface water or onto the marine coastal area, its COD should be less than 250 mg/L. Thus in the present study, the photocatalytic process did not succeed in bringing down the COD of PW to meet the discharge standards. But it did succeed in improving the biodegradability of PW. Thus a subsequent biological treatment was carried out to check if the COD could be further reduced to meet the discharge standards. The overall COD removal efficiency at the end of combined heterogeneous photocatalyst and the biological process was 41 ± 10 mg/L. Organic compounds were completely removed in 2 cycles by the biological treatment. It indicates that the sludge had high biological activity (Fig. 12).

Fig. 13 showed the morphology of active granular sludge (AGS) on day 15. It can be found from the SEM photomicrographs that there were bacilli as well as a few filamentous bacteria dominated in AGS. A closer observation of the surface of granules can show the compact structure of aerobic granules. The microorganisms were tightly linked and

Table 5
Optimization results

Optimum conditions		
pH		6.5
Time	(min)	70.26
Dosage	(g/m^2)	60
Temperature	(C)	40
H_2O_2 concentration	mM	2.5
Pred. (BOD_5/COD)		0.41
Exp. (BOD_5/COD)		0.402
Exp. COD	mg/L	1,042 ± 10
Exp. BOD	mg/L	432 ± 4

embedded with one another. Furthermore, numerous cavities were also observed in the granules. These cavities were generated along with the aggregation of bacteria cluster and could enhance the transport of oxygen and substrates into the inner cores of the granules and contributed to transferring the metabolic products out of the AGS. When aerobic granules are used for the treatment of PW, these channels can be used for transport of nutrients into the anaerobic core region of the granules.

3.4. Combined photocatalytic – biological treatment with real produced water

To examine the suitability of the proposed system for treating the real produced water, the photocatalytic system was started up with the optimum condition and according to the previous procedure. The photoreactor outlet was fed into the bioreactor with the same culture. Photoreactor performance was slightly deteriorated since the turbidity and TDS of the raw produced water was high. COD and BOD_5

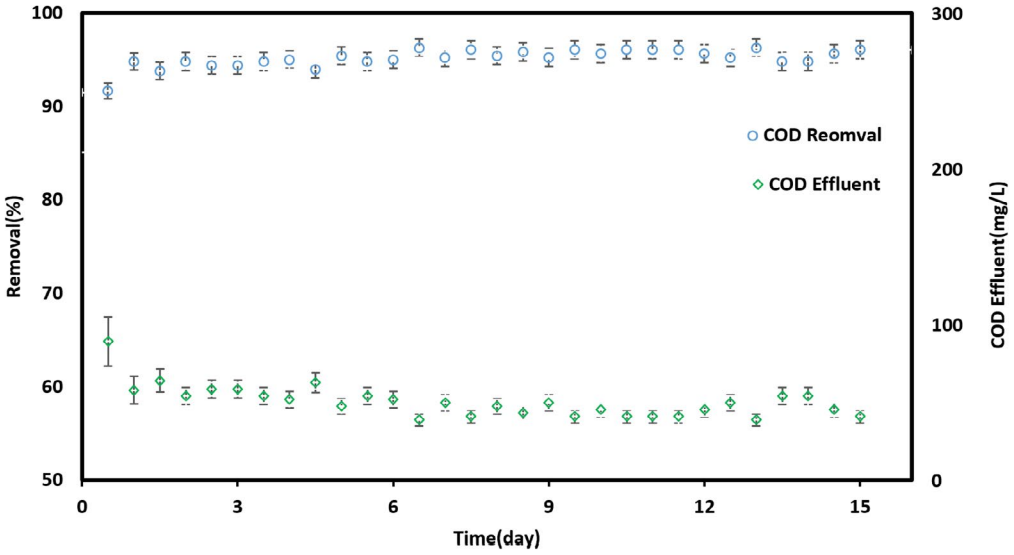

Fig. 12. BOD_5/COD ratio of effluent in integrated photoreactor – bioreactor.

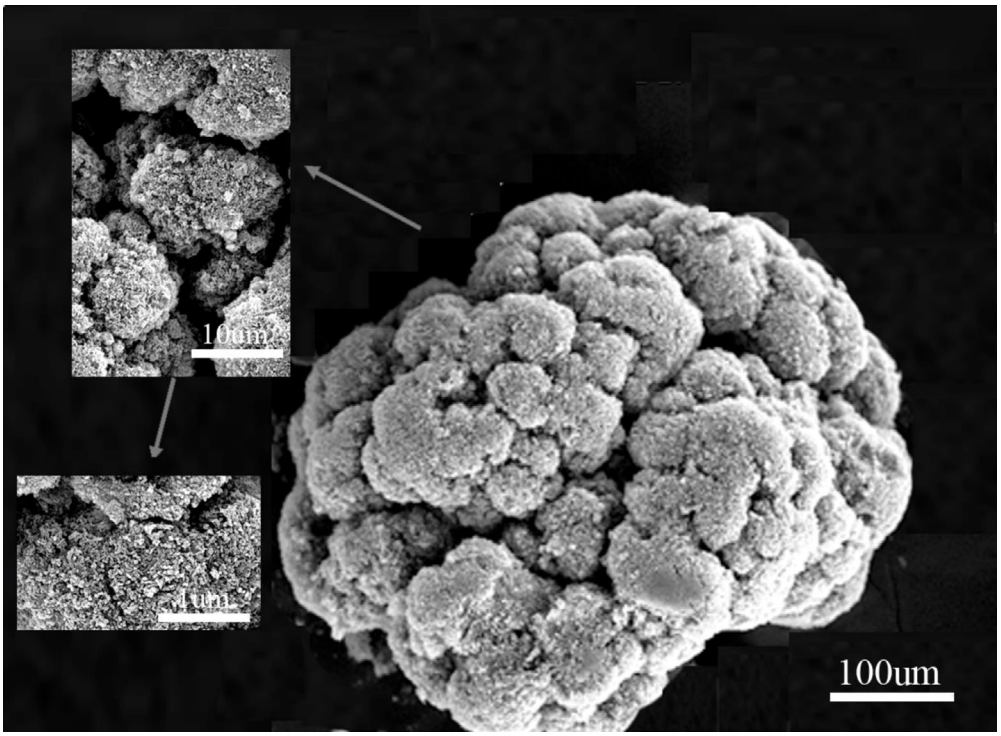

Fig. 13. SEM photomicrographs of AGS at different magnifications.

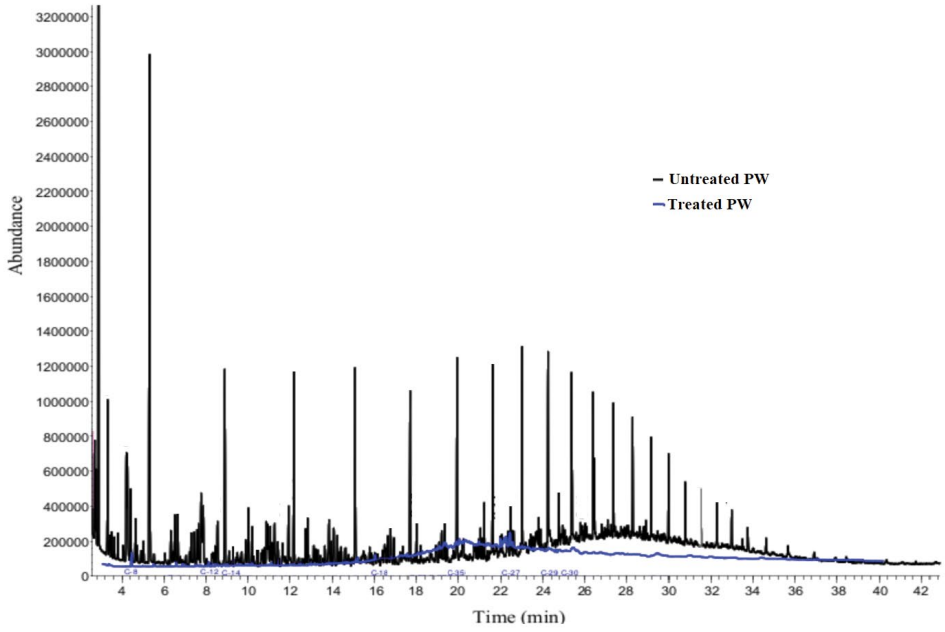

Fig. 14. GC-MS chromatograms of the PW (a) before and (b) after the treatment.

of photoreactor effluent were 1,087 and 410 mg/L , respectively. In the real produced water, the concentration of suspended oil was very low (because it was treated chemically with demulsifiers before sampling), but in the synthetic produced water, suspended hydrocarbons were dominant. The reduction of photocatalytic activity during the treatment of the real and synthetic wastewaters suggests that the presence of NaCl in the sample is responsible for the reduction of the COD removal rate. When the pre-treated real PW was fed into the bioreactor, COD removal reached to rate kept above 92%, and the effluent COD maintained under 85 ± 7 mg/L in the following time. Higher reduction of activity at higher TDS concentrations in comparison with the lower TDS concentrations, suggests that the main factor that has decreased the hydrocarbons digestion is the presence of NaCl. In this study, the results showed that increasing NaCl concentrations decreased alkanes and aromatic biodegradation in the real wastewater. GC-MS chromatograms of the untreated and treated sample under optimum conditions. The figure shows that the heavy fraction of petroleum hydrocarbons are predominant. The majority of the identified peaks consisted of aliphatic hydrocarbons, including n-branched and cycloalkanes; and polyaromatic hydrocarbons. Based on Fig. 14, a high-efficiency degradation of all organic pollutants were obtained.

4. Conclusion

The benefits of using advanced oxidation as a pre-treatment of a biological process to increase biodegradability have been proven for the treatment of wastewater. In this study, an integrated solar photoreactor – granular bioreactor was used to treat synthetic and real produced water. Solar photoreactor was designed and optimized based on cascade falling film theory. The effect of various operational parameters on the photocatalytic process was investigated by the use of RSM. Optimum BOD_5/COD ratio of 0.40 was achieved at pH of 6.5, a photocatalyst concentration of 60 g L^{-1}, temperature of 40°C, light exposure time of 70 min and H_2O_2 concentration of 2.5 mM. Photoreactor effluent with COD and BOD_5 of 1,042 ± 10 and 432 ± 4 was fed into the aerobic granular bioreactor. The removed COD by the biological treatment was 50%, whereas the combined photocatalytic–biological treatment reached 94%. In the case of real produced water, the removal efficiency was decreased to 92%. Granule structure was determined using SEM. The combined biological–photocatalytic treatment significantly shortened the degradation and mineralization time of the biological treatment.

References

[1] F.M.D. Chequer, T.M. Lizier, R. de Felício, M.V.B. Zanoni, H.M. Debonsi, N.P. Lopes, D.P. de Oliveira, The azo dye Disperse Red 13 and its oxidation and reduction products showed mutagenic potential, Toxicol. in Vitro, 29 (2015) 1906–1915.
[2] S. Munirasu, M.A. Haija, F. Banat, Use of membrane technology for oil field and refinery produced water treatment—a review, Process Saf. Environ. Prot., 100 (2016) 183–202.
[3] S. Judd, H. Qiblawey, M. Al-Marri, C. Clarkin, S. Watson, A. Ahmed, S. Bach, The size and performance of offshore produced water oil-removal technologies for reinjection, Sep. Purif. Technol., 134 (2014) 241–246.
[4] F.-R. Ahmadun, A. Pendashteh, L.C. Abdullah, D.R.A. Biak, S.S. Madaeni, Z.Z. Abidin, Review of technologies for oil and gas produced water treatment, J. Hazard. Mater., 170 (2009) 530–551.
[5] H. Mirbolooki, R. Amirnezhad, A.R. Pendashteh, Treatment of high saline textile wastewater by activated sludge microorganisms, J. Appl. Res. Technol., 15 (2017) 167–172.
[6] A.R. Pendashteh, A. Fakhru'l-Razi, N. Chaibakhsh, L.C. Abdullah, S.S. Madaeni, Z.Z. Abidin, Modeling of membrane bioreactor treating hypersaline oily wastewater by artificial neural network, J. Hazard. Mater., 192 (2011) 568–575.

[7] A. Fakhru'l-Razi, A. Pendashteh, Z.Z. Abidin, L.C. Abdullah, D.R.A. Biak, S.S. Madaeni, Application of membrane-coupled sequencing batch reactor for oilfield produced water recycle and beneficial re-use, Bioresour. Technol., 101 (2010) 6942–6949.
[8] D.H. Doyle, A.B. Brown, Produced Water Treatment and Hydrocarbon Removal with Organoclay, SPE Annual Technical Conference and Exhibition, Dallas, Texas, USA, 2000.
[9] R.M. Allen, R. Keith, Environmental Aspects of Produced Water Disposal, Paper Presented at the Middle East Oil Show, Society of Petroleum Engineers, Bahrain, 1993.
[10] R. Kendmark, M. Norozi, A. Rezaie, Biological treatment for produced water: a state of art, Environ. Toxicol. Chem., 89 (2014) 36–42.
[11] S. Jiménez, M.M. Micó, M. Arnaldos, F. Medin, S. Contreras, State of the art of produced water treatment, Chemosphere, 192 (2018) 186–208.
[12] B. Long, C.-z. Yang, W.-h. Pu, J.-k. Yang, F.-b. Liu, L. Zhang, J. Zhang, K. Cheng, Tolerance to organic loading rate by aerobic granular sludge in a cyclic aerobic granular reactor, Bioresour. Technol., 182 (2015) 314–322.
[13] N.H. Rosman, A.N. Anuar, S. Chelliapan, M.F.M. Din, Z. Ujang, Characteristics and performance of aerobic granular sludge treating rubber wastewater at different hydraulic retention time, Bioresour. Technol., 161 (2014) 155–161.
[14] B.-J. Ni, Formation, Characterization and Mathematical Modeling of the Aerobic Granular Sludge, Springer Theses, 2013, pp. 1–25.
[15] W.Q. Xue, T.W. Hao, H.R. Mackey, X.L. Li, R.C. Chan, G.H. Chen, The role of sulfate in aerobic granular sludge process for emerging sulfate-laden wastewater treatment, Water Res., 124 (2017) 513–520.
[16] S. López-Palau, A. Pinto, N. Basset, J. Dosta, J. Mata-Álvarez, ORP slope and feast–famine strategy as the basis of the control of a granular sequencing batch reactor treating winery wastewater, Biochem. Eng. J., 68 (2012) 190–198.
[17] Q.L. He, W. Zhang, S.L. Zhang, Z.C. Zou, H.Y. Wang, Performance and microbial population dynamics during stable operation and reactivation after extended idle conditions in an aerobic granular sequencing batch reactor, Bioresour. Technol., 238 (2017) 116–121.
[18] Z.W. Wang, M.C.M. van Loosdrecht, P.E. Saikaly, Gradual adaptation to salt and dissolved oxygen: strategies to minimize adverse effect of salinity on aerobic granular sludge, Water Res., 124 (2017) 702–712.
[19] T. Moustafa, Aerobic Granular Sludge – Study of Applications for Industrial and Domestic Wastewater, Master's Thesis, Department of Civil and Environmental Engineering, University of Göteborg, Sweden, 2014, p. 85.
[20] S.F. Corsino, R. Campo, G. Di Bella, M. Torregrossa, G. Viviani, Aerobic granular sludge treating shipboard slop: analysis of total petroleum hydrocarbons loading rates on performances and stability, Process Biochem., 65 (2018) 164–171.
[21] G. Di Bella, M. Torregrossa, Aerobic granular sludge for leachate treatment, J. Chem. Eng. Trans., 38 (2014) 493–498.
[22] I. Oller, S. Malato, J.A. Sánchez-Pérez, Combination of advanced oxidation processes and biological treatments for wastewater decontamination—a review, Sci. Total Environ., 409 (2011) 4141–4166.
[23] J.J. Yuan, X.K. Zhang, H.D. Li, K. Wang, S.Y. Gao, Z. Yin, H.J. Yu, X.R. Zhu, Z.Z. Xiong, Y.M. Xie, TiO_2/SnO_2 double-shelled hollow spheres-highly efficient photocatalyst for the degradation of rhodamine B, Catal. Commun., 60 (2015) 129–133.
[24] A.J. Albrbar, A. Bjelajac, V. Đjokić, J. Miladinović, D. Janaćković, R. Petrović, Photocatalytic efficiency of titania photocatalysts in saline waters, J. Serb. Chem. Soc., 79 (2014) 1127–1140.
[25] R. Nadarajan, W.A.W.A. Bakar, R. Ali, R. Ismail, Photocatalytic degradation of 1,2-dichlorobenzene using immobilized TiO_2/SnO_2/WO_3 photocatalyst under visible light: application of response surface methodology, Arabian J. Chem., 11 (2018) 34–47.
[26] S. Malato, J. Blanco, J. Cáceres, A.R. Fernández-Alba, A. Agüera, A. Rodríguez, Photocatalytic treatment of water-soluble pesticides by photo-Fenton and TiO_2 using solar energy, Catal. Today, 76 (2002) 209–220.
[27] S. Malato, J. Blanco, D.C. Alarcón, M.I. Maldonado, P. Fernández-Ibáñez, W. Gernjak, Photocatalytic decontamination and disinfection of water with solar collectors, Catal. Today, 122 (2007) 137–149.
[28] S. Malato, P. Fernández-Ibanez, M.I. Maldonado, J. Blanco, W. Gernjak, Decontamination and disinfection of water by solar photocatalysis: recent overview and trends, Catal. Today, 147 (2009) 1–59.
[29] S. Malato, J. Blanco, A. Vidal, D. Alarcón, M.I. Maldonado, J. Cáceres, W.G. Gernjak, Applied studies in solar photocatalytic detoxification: an overview, Sol. Energy, 75 (2013) 329–336.
[30] C. Minero, E. Pelizzetti, S. Malato, J. Blanco, Large solar plant photocatalytic water decontamination: degradation of pentachlorophenol, Chemosphere, 26 (1993) 2103–2119.
[31] W. Gernjak, M.L. Maldonado, S. Malato, J. Cáceres, T. Krutzler, A. Glaser, R. Bauer, Pilot-plant treatment of olive mill wastewater (OMW) by solar TiO_2 photocatalysis and solar photo-Fenton, Sol. Energy, 77 (2004) 567–572.
[32] A. Vidal, A.I. Díaz, A. El Hraiki, M. Romero, I. Muguruza, F. Senhaji, J. González, Solar photocatalysis for detoxification and disinfection of contaminated water: pilot plant studies, Catal. Today, 54 (1999) 283–290.
[33] M.C. Liu, D.W. Jing, L. Zhao, L.J. Guo, Preparation of novel CdS-incorporated special glass composite as photocatalyst material used for catalyst-fixed system, Int. J. Hydrogen Energy, 35 (2010) 7058–7064.
[34] D.W. Jing, H. Liu, X.H. Zhang, L. Zhao, L.J. Guo, Photocatalytic hydrogen production under direct solar light in a CPC based solar reactor: reactor design and preliminary results, Energy Convers. Manage., 50 (2009) 2919–2926.
[35] F. Cao, Q.Y. Wei, H. Liu, N. Lu, L. Zhao, L.J. Guo, Development of the direct solar photocatalytic water splitting system for hydrogen production in Northwest China: design and evaluation of photoreactor, Renewable Energy, 121 (2018) 153–163.
[36] Q.Y. Wei, Y. Yang, J.Y. Hou, H. Liu, F. Cao, L. Zhao, Direct solar photocatalytic hydrogen generation with CPC photoreactors: system development, Sol. Energy, 153 (2017) 215–223.
[37] S. Malato, J. Blanco, A. Vidal, C. Richter, Photocatalysis with solar energy at a pilot-plant scale: an overview, Appl. Catal., B, 37 (2002) 1–15.
[38] S. Malato, J. Blanco, C. Richter, D. Curcó, J. Giménez, Low-concentrating CPC collectors for photocatalytic water detoxification: comparison with a medium concentrating solar collector, Water Sci. Technol., 35 (1997) 157–164.
[39] Sutisna, M. Rokhmat, E. Wibowo, Khairurrijal, M. Abdullah, Prototype of a flat-panel photoreactor using TiO_2 nanoparticles coated on transparent granules for the degradation of Methylene Blue under solar illumination, Sustainable Environ. Res., 27 (2017) 172–180.
[40] C. Casado, Á. García-Gil, R. van Grieken, J. Marugán, Critical role of the light spectrum on the simulation of solar photocatalytic reactors, Appl. Catal., B, 252 (2019) 1–9.
[41] L. Onotri, M. Race, L. Clarizia, M. Guida, M. Alfè, R. Andreozzi, R. Marotta, Solar photocatalytic processes for treatment of soil washing wastewater, Chem. Eng. J., 318 (2017) 10–18.
[42] L. Aoudjit, P.M. Martins, F. Madjene, D.Y. Petrovykh, S. Lanceros-Mendez, Photocatalytic reusable membranes for the effective degradation of tartrazine with a solar photoreactor, J. Hazard. Mater., 344 (2018) 408–416.
[43] K. Sofía Ochoa-Gutiérrez, E. Tabares-Aguilar, M. Ángel Mueses, F. Machuca-Martínez, G.L. Puma, A novel prototype offset multi tubular photoreactor (OMTP) for solar photocatalytic degradation of water contaminants, Chem. Eng. J., 341 (2018) 628–638.
[44] P. Jain, M. Sharma, P. Dureja, P.M. Sarma, B. Lal, Bioelectrochemical approaches for removal of sulfate, hydrocarbon and salinity from produced water, Chemosphere, 166 (2017) 96–108.
[45] D. Suryaman, K. Hasegawa, Biological and photocatalytic treatment integrated with separation and reuse of titanium dioxide on the removal of chlorophenols in tap water, J. Hazard. Mater., 183 (2010) 490–496.

[46] M.P. Shah, Combined application of biological-photocatalytic process in degradation of reactive black dye: an excellent outcome, Am. J. Microbiol. Res., 4 (2013) 92–97.
[47] M.P. Reddy, B. Srinivas, V.D. Kumari, M. Subrahmanyam, P.N. Sharma, An integrated approach of solar photocatalytic and biological treatment of N-containing organic compounds in wastewater, Toxicol. Environ. Chem., 86 (2004) 127–140.
[48] A. Baiju, R. Gandhimathi, S.T. Ramesh, P.V. Nidheesh, Combined heterogeneous Electro-Fenton and biological process for the treatment of stabilized landfill leachate, J. Environ. Manage., 210 (2018) 328–337.
[49] F. Martínez, R. Molina, I. Rodríguez, M.I. Pariente, Y. Segura, J.A. Melero, Techno-economical assessment of coupling Fenton/biological processes for the treatment of a pharmaceutical wastewater, J. Environ. Chem. Eng., 6 (2019) 485–494.
[50] C.Y. Chan, H.S. Chan, P.K. Wong, Integrated photocatalytic-biological treatment of triazine-containing pollutants, Chemosphere, 222 (2019) 371–380.
[51] V. Bhatia, A. Dhir, A.K. Ray, Integration of photocatalytic and biological processes for treatment of pharmaceutical effluent, J. Photochem. Photobiol., A, 364 (2018) 322–327.
[52] M. Wu, J. Deng, J. Li, Y. Li, J. Li, H. Xu, Simultaneous biological-photocatalytic treatment with strain CDS-8 and TiO_2 for chlorothalonil removal from liquid and soil, J. Hazard. Mater., 320 (2016) 612–619.
[53] Y.M. Zhang, L. Wang, B.E. Rittmann, Integrated photocatalytic-biological reactor for accelerated phenol mineralization, Appl. Microbiol. Biotechnol., 86 (2010) 1977–1985.
[54] E.-S. Kim, G. Hwang, M.G. El-Din, Y. Liu, Development of nanosilver and multi-walled carbon nanotubes thin-film nanocomposite membrane for enhanced water treatment, J. Membr. Sci., 394–395 (2012) 37–48.
[55] M.D. Marsolek, M.J. Kirisits, K.A. Gray, B.E. Rittmann, Coupled photocatalytic-biodegradation of 2,4,5-trichlorophenol: effects of photolytic and photocatalytic effluent composition on bioreactor process performance, community diversity, and resistance and resilience to perturbation, Water Res. , 50 (2014) 59–69.
[56] A.R. Pendashteh, L.C. Abdullah, A. Fakhru'l-Razi, S.S. Madaeni, Z.Z. Abidin, D.R.A. Biak, Evaluation of membrane bioreactor for hypersaline oily wastewater treatment, Process Saf. Environ. Prot., 90 (2012) 45–55.
[57] M. Delnavaz, Photo catalysis of Wastewater Containing Phenol mediated by Nano TiO_2 Fixed to Concrete Surfaces, Department of Environmental Engineering & Faculty of Civil and Environmental Engineering, Tarbiat Modares University, 2011.
[58] M. Delnavaz, B. Ayati, H. Ganjidoust, S. Sanjabi, Kinetics study of photocatalytic process for treatment of phenolic wastewater by TiO_2 nano powder immobilized on concrete surfaces, Toxicol. Environ. Chem., 94 (2012) 1086–1098.
[59] E.W. Rice, R.B. Baird, A.D. Eaton, Standard Methods for the Examination of Water & Wastewater, American Public Health Association, American Water Works Association, and Water Environment Federation, USA, 2017.
[60] D.D.C. Freire, G.L. Sant'Anna, A proposed method modification for the determination of cod in saline waters, Environ. Technol., 19 (1998) 1243–1247.
[61] D.D.C. Freire, M.C. Cammarota, G.L. Sant'Anna, Biological treatment of oil field wastewater in a sequencing batch reactor, Environ. Technol., 22 (2001) 1125–1135.
[62] Standard Method for Examination of Water and Wastewater, 19th ed., APHA, AWWA, WEF, Washington, D.C., USA, 2005.
[63] M. Alizadeh, S.M. Sadrameli, Indoor thermal comfort assessment using PCM based storage system integrated with ceiling fan ventilation: experimental design and response surface approach, Energy Build., 188–189 (2019) 297–313.
[64] M. Alizadeh, S.M. Sadrameli, Numerical modeling and optimization of thermal comfort in building: central composite design and CFD simulation, Energy Build., 164 (2018) 187–202.
[65] Z. Ghasemi, H. Younesi, A.A. Zinatizadeh, Preparation, characterization and photocatalytic application of TiO_2/Fe-ZSM-5 nanocomposite for the treatment of petroleum refinery wastewater: optimization of process parameters by response surface methodology, Chemosphere, 159 (2016) 552–564.
[66] S. Khodadoust, A. Sheini, N. Armand, Photocatalytic degradation of monoethanolamine in wastewater using nanosized TiO_2 loaded on clinoptilolite, Spectrochim. Acta, Part A, 92 (2012) 91–95.
[67] S. Ahmed, M.G. Rasul, W.N. Martens, R. Brown, M.A. Hashib, Heterogeneous photocatalytic degradation of phenols in wastewater: a review on current status and developments, Desalination, 261 (2010) 3–18.
[68] C.-H. Chiou, R.-S. Juang, Photocatalytic degradation of phenol in aqueous solutions by Pr-doped TiO_2 nanoparticles, J. Hazard. Mater., 149 (2007) 1–7.
[69] J. Saien, H. Nejati, Enhanced photocatalytic degradation of pollutants in petroleum refinery wastewater under mild conditions, J. Hazard. Mater., 148 (2007) 491–495.
[70] A. Aleboyeh, Y. Moussa, H. Aleboyeh, The effect of operational parameters on UV/H_2O_2 decolourisation of Acid Blue 74, Dyes Pigm., 66 (2005) 129–132.
[71] C.C. Wong, W. Chu, The hydrogen peroxide-assisted photocatalytic degradation of alachlor in TiO_2 suspensions, Environ. Sci. Technol., 37 (2003) 2310–2316.
[72] D.-H. Tseng, L.-C. Juang, H.-H. Huang, Effect of oxygen and hydrogen peroxide on the photocatalytic degradation of monochlorobenzene in TiO_2 aqueous suspension, Int. J. Photoenergy, 2012 (2012) 9 p, http://dx.doi.org/10.1155/2012/328526.
[73] D.D. Dionysiou, M.T. Suidan, E. Bekou, I. Baudin, J.M. Laîné, Effect of ionic strength and hydrogen peroxide on the photocatalytic degradation of 4-chlorobenzoic acid in water, Appl. Catal., B, 26 (2000) 153–171.
[74] Y.J. Zang, R. Farnood, Effect of hydrogen peroxide on the photocatalytic degradation of methyl *tert*-butyl ether, Top. Catal., 37 (2006) 91–96.
[75] I. Talinli, G.K. Anderson, Interference of hydrogen peroxide on the standard COD test, Water Res., 26 (1992) 107–110.
[76] Y.K. Abdel-Maksoud, E. Imam, A. Ramadan, TiO_2 solar photocatalytic reactor systems: selection of reactor design for scale-up and commercialization, Catalysts, 6 (2016) 138–142.